



Enhanced photovoltaic performance and morphological control of PbS CE grown on functionalized self-assembly nanocrystals for quantum-dot sensitized solar cells via cost-effective chemical bath deposition

Journal:	<i>Journal of Materials Chemistry C</i>
Manuscript ID:	TC-ART-07-2015-001988.R1
Article Type:	Paper
Date Submitted by the Author:	22-Aug-2015
Complete List of Authors:	Venkata Tulasivarma, Ch; Pusan National University, Rao, S; Pusan National University, Electrical Engineering Ikkurthi, Kanaka Durga; Pusan National University, Electrical Engineering Kim, Soo-Kyoung; Pusan National University, Electrical Engineering Kang, Tae-Su; Pusan National University, Electrical Engineering Kim, Heeje; Pusan National University, Electrical Engineering; Home,

Enhanced photovoltaic performance and morphological control of PbS counter electrode grown on functionalized self-assembly nanocrystals for quantum-dot sensitized solar cells via cost-effective chemical bath deposition.

Chebrolu Venkata Thulasi-Varma, S. Srinivasa Rao, I Kanaka Durga, Soo-Kyoung Kim, Tae-Su Kang, Hee-Je Kim*

School of Electrical Engineering, Pusan National University, Gumjeong-Ku, Jangjeong-Dong, Busan 609-735, South Korea

*Corresponding author. Tel.: +82 51 510 2364; fax: +82 51 513 0212.

E-mail address: heeje@pusan.ac.kr (H.-J. Kim).

†Electronic supplementary information (ESI) available: Dark current Vs potential curves of QDSSCs with different counter electrodes under dark condition, Additional characterization data from CV analysis of PbS and Pt CEs, Parameters of the quantum dot-sensitized solar cell using with different thickness as counter electrodes measured under AM 1.5 illumination, PbS CE sheet resistance Vs thickness are shown in Fig S1, S2, S3, and S4.

Abstract:

This study describes the synthesis of monodispersed PbS nanocrystals by a facile chemical bath deposition and cost-effective approach. PbS counter electrodes (CEs) were used to grow high-quality thin films containing cube-shaped nanocrystals or nanodendrites. The size and shape of the PbS nanocrystals can be easily controlled by varying the deposition time. Quantum dot-sensitized solar cells (QDSSCs) were made and showed improved performance using the PbS CE obtained with a deposition time of 2 h. The nanocrystal structured PbS CE in QDSSCs under one-sun illumination (AM 1.5, 100 Mw cm⁻²) yielded a high short circuit current density (J_{SC}) of 11.20 mA cm⁻², open circuit voltage (V_{oc}) of 0.560 V, fill Factor (FF) of 0.55, and power

conversion efficiency (η) of 3.48 %. These values are much higher than those of the Pt CE ($J_{SC}=79.29 \text{ mA cm}^{-2}$, $V_{oc}=0.604$, $FF=0.28$, and $\eta=1.58 \%$). The concentration of acetic acid plays an important role in deciding the size and shape of the PbS nanocrystals in the nucleation and growth process. The PbS strongly adhered to the FTO substrate due to the acetic acid, which acts as a stabilizer and strong reagent in this one-step preparation. The performance of PbS CE was improved by the surface morphology, which enables rapid electron transport and a lower electron recombination rate for the polysulfide electrolyte redox couple. Electrochemical impedance spectroscopy and Tafel-polarization measurements were used to investigate the electrocatalytic activity of the PbS and Pt CEs.

1. Introduction

The current energy crisis caused by over usage of fossil fuels has led to environmental pollution, fuel depletion, and global warming.¹⁻³ Therefore, many researchers have paid significant attention to developing green and sustainable renewable energy sources. In the past few years Quantum dot –sensitized solar cells (QDSSCs) represents a one of the new photovoltaic devices that could create as a promising requirements of third generation solar cells, due to their unique advantages over conventional dyes such as QDs as photon harvesters, which include a strong photo-response in the visible region, high extinction coefficients, large intrinsic dipole moment, and easily tunable band gap compared to organic dye³⁻⁸ based on the multiple exciton generation of QDs.^{9, 4, 5} In addition, quantum dots (QDs) have hot carrier transfer properties as light absorbers that leads to rapid charge separation.

The QDSSC structure is similar to that of dye-sensitized solar cells (DSSCs), and QDSSC fabrication is cost-effective and simple. Generally, QDSSCs are composed of a wide-

bandgap semi-conductor photoelectrode, sensitizer, redox electrolyte, and counter electrode (CE). In the past decade, great efforts have been made to improve the energy conversion efficiency of QDSSCs using various strategies. Generally, there are few routes to improve the performance of QDSSCs: (1) design and optimization of QD deposition on TiO₂ film,¹⁰⁻¹⁵ (2) morphological and nanostructural modification of the photosensitive materials and the substrate, (3) componential modification of the photosensitive materials and substrate with chemical doping, adding chemical compounds, or using new kinds of QD sensitizers.^{16, 17, 18}

Recently, an impressive energy conversion efficiency of 8% was achieved with recombination control of QDSSCs.¹⁹ However, the photovoltaic performance of QDSSCs is still very low compared to DSSCs due to inefficient charge separation and transfer at the various interfaces.²⁰⁻²⁴ The CE and polysulfide electrolyte in QDSSCs are correspondingly important. Poor charge transfer oxidized polysulfide redox species (S_n^{2-}) on CEs is considered to be a major hurdle in attaining a high fill factor and conversion efficiency in QDSSCs.^{23, 25}

In DSSCs, Pt has exhibited excellent electro-catalytic activity due to its stability for the reduction of I_3^- , but Pt is not suitable for QDSSCs because it causes rapid corrosion and photodegradation of the QDs.²⁶ The Pt CE usually achieved very low fill factor and conversion efficiency in QDSSCs, resulting in over potential for regeneration of the polysulfide electrolyte owing to the chemisorption of sulfur compounds on the Pt surface. To accomplish efficient charge separation in QDSSCs, regenerative polysulfide electrolyte (S^{2-}/S_x^{2-}) is more compatible with the sulfide sensitizer. Therefore, an aqueous polysulfide electrolyte is usually used in QDSSCs. This electrolyte shows strong selectivity toward the CE.

The series resistance is one of the key parameters in both DSSCs and QDSSCs. Efficient charge transfer between the sulfide sensitizers and polysulfide electrolyte results in high charge short-circuit current density (J_{SC}) in QDSSCs as a result of a low fill factor. To improve the fill factor and conversion efficiency of QDSSCs, several new CE materials have been studied for QDSSCs to replace Pt CEs, such as Cu_2S , CoS , NiS , PbS , CuS ,^{23, 28-35} carbon materials,^{36, 37} and conducting polymers.³⁸ Among these CEs, the best results were achieved by metal sulfides, especially Cu_2S CEs show outstanding catalytic activity and good electrical properties.²³ However, the studies and preparation methods for metal sulfide CEs have been inadequate. The preparation of metal sulfide CEs involves direct immersion into sulfide solution to obtain an interfacial layer of metal sulfides.³⁹ Such CEs suffer from continual corrosion and mechanical instability and will completely disintegrate in the presence of sulfide/polysulfide electrolyte.⁴⁰ To solve this problem, we have turned our attention to seeking cheaper and simpler methods.

Various deposition methods have been applied to deposit metal sulfides on FTO or ITO glass, such as electrode deposition,⁴¹ successive ionic layer adsorption and reaction (SILAR),⁴² hydrothermal methods,⁴³ proximal (or direct) adsorption,⁴⁴ and chemical bath deposition (CBD).⁴⁵ CBD has gained popularity due to its simplicity and, more importantly, the intimate contact between the donors and acceptors, through which QDs are formed directly on the substrate by ionic species from precursor solutions. However, despite these advantages, new CE materials are required to further enhance the power conversion efficiency (PCE) of QDSSCs and achieve high stability, high electrocatalytic activity, and consistent performance in sulfide/polysulfide electrolyte.

Lead sulfide (PbS) is a P-type semi-conductor that has attracted considerable attention for use in QDSSCs and perovskite solar cells. PbS has promising stability and good catalytic activity

in the near-infrared region (NIR). We report on PbS grown in situ on FTO glass substrates by a simple and cost-effective CBD method using acetic acid and different deposition times. An energy conversion efficiency of 3.48% was achieved using simple and inexpensive materials. This is the best efficiency achieved using acetic acid for PbS CEs in QDSSCs so far.^{46, 47} To the best of our knowledge, this promising PbS CE using acetic acid with different deposition times has not been used in polysulfide electrolyte previously. The photovoltaic performance is improved by the excellent electron transport from an external circuit, and as a result, electrons are used to oxidize the polysulfide electrolyte. The high electrocatalytic activity of the PbS CE significantly improves the surface morphology and energy conversion efficiency.

The transport pathways of electrons and photoelectrical conversion configuration of a $\text{TiO}_2/\text{CdS}/\text{CdSe}/\text{ZnS}$ based QDSSCs with nanocrystal structure of PbS CE as described in Fig. 1. The configuration consists of a photoanode $\text{TiO}_2/\text{CdS}/\text{CdSe}/\text{ZnS}$ QD sensitizer, polysulfide electrolyte and FTO/PbS CE. As shown in schematic diagram, under one sun illumination (100 mW cm^{-2}) upon photo-excitation of the QD's, yielding the electron-hole pairs at the interface between the nanocrystalline oxide and QDs. The electrons are injected from the excited state of CdS/CdSe/ZnS QDs into TiO_2 and finally to the FTO and the holes are concurrently oxidizing the polysulfide electrolyte through the reaction of $nS^{2-} + h^+ \rightarrow S_n^{2-}$. The electrons in the FTO moved to the cathode via hole transporting of redox couple of the polysulfide electrolyte and participates in the reduction reaction of CEs/electrolyte interface, $S_n^{2-} + e^- \rightarrow nS^{2-}$. As a result an ideal PbS CE should possess high electro catalytic activity and conductivity for the reduction of charge carriers in the electrolyte.

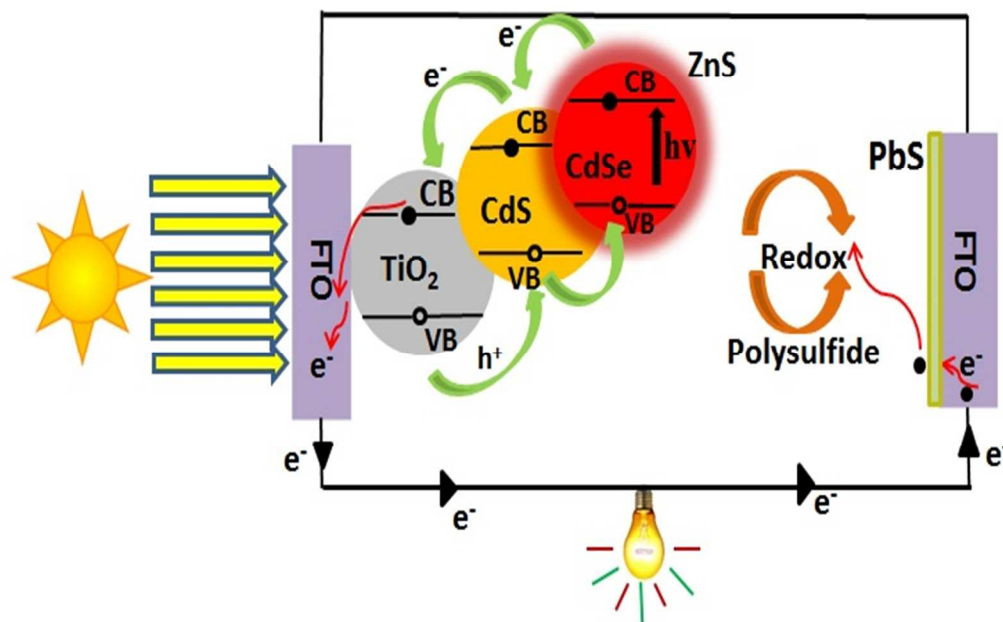


Fig. 1 Schematic structure of $\text{TiO}_2/\text{CdS}/\text{CdSe}/\text{ZnS}$ QDSSC based nanocrystal structure of PbS CE.

2. Experimental section

2.1 Materials

The following chemicals were purchased from Sigma-Aldrich: lead nitrate ($\text{Pb}(\text{NO}_3)_2$), thioacetamide ($\text{C}_2\text{H}_5\text{NS}$, 99.0%), acetic acid ($\text{C}_2\text{H}_4\text{O}_2$), cadmium acetate ($\text{Cd}(\text{CH}_3\text{COO} \cdot 2\text{H}_2\text{O})$), sodium sulfide ($\text{Na}_2\text{S} \cdot 9\text{H}_2\text{O}$), sodium sulfite (Na_2SO_3), selenium (Se) (100 mesh 99.5%), zinc acetate ($(\text{CH}_3\text{CO}_2)_2\text{Zn}$, 99%), potassium chloride (KCl), and TiO_2 paste (Ti-nanoxide HT/SP). All chemicals were used directly without further purification.

2.2. Preparation of PbS and Pt CEs

The PbS CEs were deposited on FTO substrates with a sheet resistance of $7 \Omega/\text{cm}^2$. Prior to deposition, the FTO substrates were well cleaned ultrasonically with acetone, ethanol, and

deionized (DI) water for 10 minutes each. Briefly, $(\text{Pb}(\text{NO}_3)_2)$ was used as a lead precursor, $\text{C}_2\text{H}_5\text{NS}$ was used as a sulfur source, and acetic acid was used as a reagent in the deposition. Acetic acid acts as a stabilizer, complexing agent and enriches the S^{2-} concentration versus S atoms in the preparation process. No-visible coating was observed on the FTO substrates without acetic acid. In 25 ml of deionized water (DI), 0.1 M $\text{Pb}(\text{NO}_3)_2$ was dissolved under magnetic stirring. Then, 0.4 M $\text{C}_2\text{H}_5\text{NS}$ was added to the solution and vigorously stirred for about 30 min to obtain a transparent solution. Afterward, the two transparent solutions were mixed together with slow stirring. Finally, 0.7 ml of acetic acid was added to the precursor solution drop by drop under vigorous stirring for about 1 hr.

The well-cleaned FTO substrates were immersed horizontally in the growth solution and placed in a hot air oven. The deposition was carried out at a constant temperature of 90°C for time periods of 1.5 h, 2 h, 2.5 h, and 3 h, and the PbS CEs were denoted as PbS 1.5 h, PbS 2 h, PbS 2.5 h, and PbS 3 h, respectively. When the deposition time was 3 h, the PbS-coated substrates peeled off from the film, so further experiments were done with PbS CEs using deposition times of 1.5 h, 2 h, and 2.5 h. After the deposition, the PbS-coated thin films were removed from the oven and cooled to room temperature. After cooling, the PbS-coated FTO substrates were rinsed with DI water and ethanol and dried with an air stream.

For comparison, we prepared commercial Pt paste (Solaronix, platinum catalyst T/SP), applied it to well-cleaned FTO substrates using the doctor blade method, and heat-treated it at 450°C for 10 min in air.

2.3 Synthesis of working electrode (TiO₂/CdS/CdSe/ZnS):

Prior to preparation of photoanodes a SILAR technique was used to fabricate QD-sensitized photoanodes.⁴⁸ FTO substrates were ultrasonically cleaned with acetone, ethanol, and DI water for 10 min each. Briefly, commercial porous TiO₂ paste with a particle size of 20 nm (Ti-Nanoxide HT/TP, Solaronix) was coated on FTO glass by the doctor blade method and sintered at 450°C for 30 minutes. After solvent evaporation, the thickness was 7.5 μm with an active area of 0.27 cm².

Electrode sensitization

TiO₂ nanostructured electrodes were sensitized by CdS QDs directly grown on the photoelectrode surface. For the preparation of CdS QDs, anionic (Cd²⁺) and cationic (S²⁻) ion sources were prepared with 0.1 M Cd(CH₃COO)₂ and 0.1 M Na₂S, respectively. First, the TiO₂ electrodes were immersed in an aqueous solution of Cd(CH₃COO)₂·2H₂O for 5 minutes to allow the Cd²⁺ ions to coat the TiO₂ electrode. The film was rinsed with DI water and ethanol for 1 min to remove the excess Cd²⁺ ions and dried under N₂ gas. The adsorbed anionic (Cd²⁺) photoanodes were then dipped into the Na₂S solution for about 5 minutes for the cations (S²⁻) to adsorb and react with the anions (Cd²⁺) to form CdS QDs. This was followed by sublimation with DI water and ethanol, removal of the anions, and drying with N₂ gas. This two-step dipping procedure is considered as one cycle. The process was repeated for 5 cycles at room temperature to achieve good adhesion on the substrate. The as-prepared electrodes are denoted as TiO₂/CdS₅ photoanodes.

For the deposition of CdSe, 0.1 M of Cd(CH₃COO)₂ and Se sources were used for 8 alternate dipping cycles with the SILAR method. For the preparation of Se, a reflexing technique

was used with an aqueous solution of 0.2 M of Se and 0.4 M of Na_2SO_3 at 120°C for 4 h. The as-prepared photo-anodes are denoted as $\text{TiO}_2/\text{CdS}_5/\text{CdSe}_8$ electrodes. Finally, a ZnS passivation layer was deposited on the $\text{CdS}_5/\text{CdSe}_8$ layer using the SILAR method with an aqueous solution of 0.1 M of $\text{Zn}(\text{CH}_3\text{COO})_2 \cdot 2\text{H}_2\text{O}$ and 0.1 M of Na_2S applied for 1 minute for about 2 cycles. This was followed by washing with DI water and ethanol alternately and drying with N_2 gas.

The use of wide-band-gap semiconductors (typically ZnS) as passivation layers on QD sensitizers can efficiently decrease the rate of recombination and assist in electron transport in the presence of polysulfide electrolyte.⁴⁹ Moreover, the ZnS passivation layer can further increase the efficiency of QDSSCs. The QD-adsorbed TiO_2 electrodes and the CuS and Pt CEs were assembled at 100°C using a hot melting sheet (SX 1170-60, Solaronix). The internal space was filled by capillary action with a redox liquid electrolyte containing 1 M Na_2S with 2 M S and 0.2 M KCl in methanol and DI water at a ratio of 7:3. The CEs were covered with the sealant and cover glass and then soldered. The cells were left for a few minutes for complete diffusion of the electrolyte within the photoanode and finally tested under $\sim 100 \text{ mW cm}^{-2}$ illumination.

2.4 Fabrication of symmetric cells for EIS and Tafel analysis.

The symmetrical CEs of PbS and Pt were assembled using a hot melting sheet (SX 1170-60, Solaronix) at 100°C , and the internal space was filled with a redox liquid electrolyte containing 1 M Na_2S with 2 M S and 0.2 M KCl in methanol and DI water at a ratio of 7:3. Electrochemical impedance spectroscopy (EIS) and Tafel measurements were carried out using a Biologic potentiostat/galvanostat/EIS analyzer (SP-150, France) with a scan rate of 10 mVs^{-1} for the symmetrical dummy cells of PbS and Pt CEs under dark conditions in a frequency range of 100 mHz to 500 kHz.

2.5 Characterization techniques.

The crystal nature and structure of the PbS thin films was characterized by powder X-ray diffraction (XRD) on a D8 ADVANCE with a Cu K α radiation source ($\lambda=1.54060$) operated at 40 kV and 40 mA in the range 20° to 80°. The surface morphology, thickness, and elemental compositions of the PbS CE thin films were estimated using a field emission scanning electron microscope (FE-SEM, SU-70, and Hitachi) operated at 10.0 kV, respectively. The surface roughness of the PbS FTO substrate was characterized by atomic force microscope (JPK NanoWizard II AFM, JPK Instruments, Berlin, Germany) with a scan rate of 0.8 Hz in contact mode.

The current-voltage (J-V) characteristics of the QDSSCs were obtained under one-sun illumination (AM 1.5G, 100 mW cm⁻²) using an ABET technologies solar simulator (USA) with an irradiance constancy of $\pm 3\%$. Electrochemical impedance spectroscopy (EIS) was done using a Biologic potentiostat/galvanostat/EIS analyzer (SP-150, France) under one-sun illumination with a frequency range of 100 mHz to 500 kHz. Tafel polarization (scan rate 10 mV s⁻¹) was also performed for the symmetrical cells of PbS/PbS and Pt/Pt CEs in dark conditions. To better understand the electrocatalytic activity of PbS CEs, cyclic voltammetry was performed using three electrode system.

3. Results and discussion

Fig. 2 shows the XRD diffraction patterns of PbS thin films obtained from CBD under optimum deposition conditions from 1.30 h to 2.30 h. The diffraction peaks observed at diffraction angles (2θ) of 25.9°, 43.1°, 51.0°, 53.4°, 62.5°, 68.9°, 71.0°, 79.0°, and 84.8° respectively corresponded to the [111], [220], [311], [222], [400], [331], [422], and [511] miller planes of the PbS with face-centered cubic structure. These values are in good agreement with

the standard X-ray diffraction data file (PDF No. 650135). The appearance of sharp peaks indicates polycrystalline nature of the film.

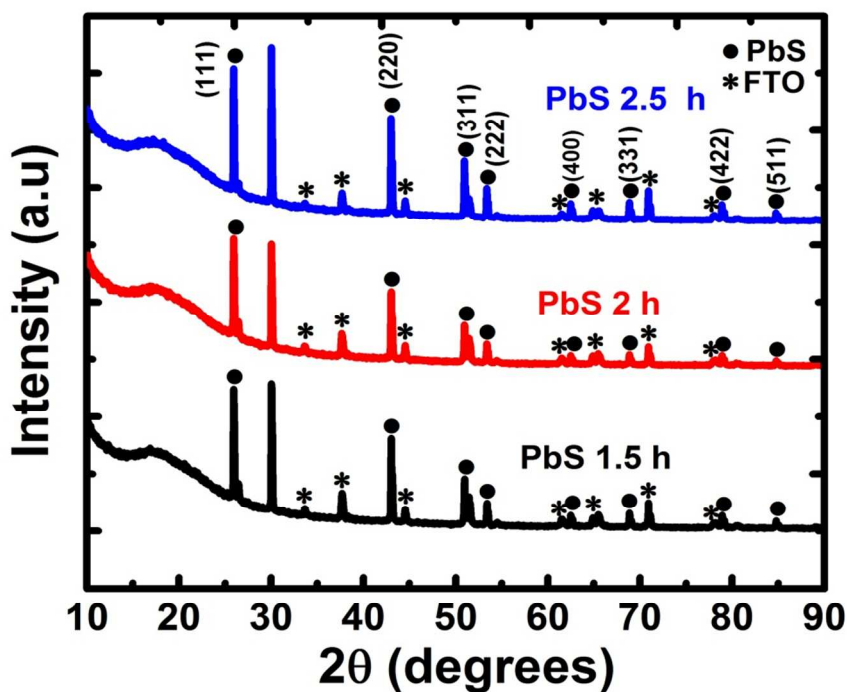


Fig. 2 X-ray diffraction spectrum of PbS thin films deposited on FTO substrates

High-quality PbS nanocrystals formed when the deposition time was over 1.5 h. The intensity of the diffraction peaks gradually decreases for 2 h of deposition compared to 1.5 h and 2.5 h. This suggests that the thickness of PbS nanocrystals increases with increasing the deposition time from 1.5 h to 2 h. The XRD results consistent with the SEM images. The highest intensities were noted for the [111] and [220] planes, indicating that the nanocrystals have a preferential coordination towards the [111] and [220] directions that depends on the deposition time.

The absence of any other prominent diffraction peaks in the XRD analysis indicates that there are no other crystalline phases such as PbO or PbSO₄. However, deposition time over 2.5

h may lead to uncontrolled growth of nanocrystals and make it difficult to exploit suitable kinetic or energetic effects to achieve precise control over the size and size distribution of nanocrystals. From the SEM and XRD analysis, we can conclude that the optimized deposition time greatly affects the phase formation of PbS nanocrystals.

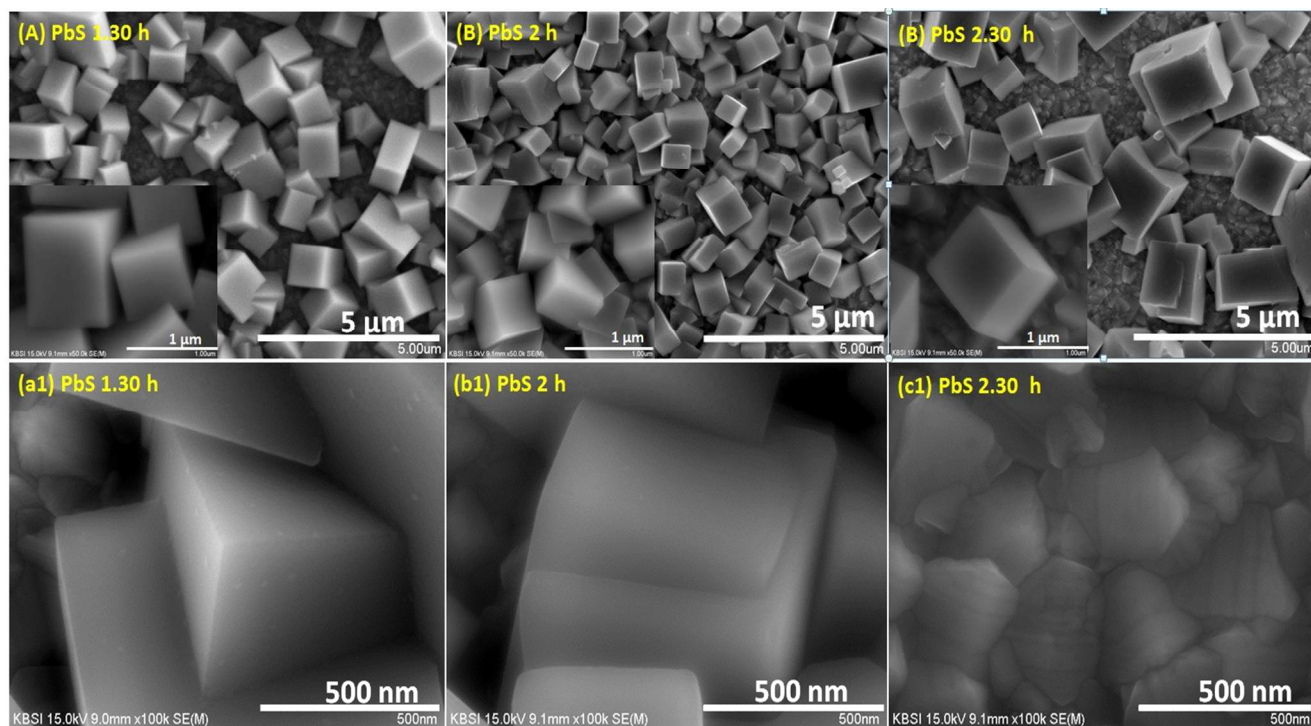


Fig. 3 SEM images of PbS thin films deposited on FTO substrates with different deposition times.

Fig. 3 shows the SEM images at low magnification and high magnification of PbS nanocrystal thin films prepared at different deposition times via CBD. The deposition time of PbS 2 h film have uniform surface morphology and good quality over the entire FTO substrate without any empty surface regions. The deposition times played an important role in the formation of PbS nanocrystals in the presence of acetic acid. The formation of PbS on FTO substrate was not observed when the deposition time was less than 1 h. As shown in the SEM images, nanocrystals formed when the deposition time was 1.5 h, and the film thickness was about 734 nm. When the deposition time increased to 2 h, more cube-shaped nanocrystals were

obtained, the distance between the crystals was reduced, and the crystals formed aggregates of denser crystals. The film thickness also gradually increased from 734 nm to 1.32 μm . This indicates that along with the increasing deposition time, the diffusion velocity of crystals in the system was accelerated and their porosity declined due to the aggregation of the crystals.

After 2 h, the film had improved morphology, as shown in Fig. 3b, which may increase the electrocatalytic activity to efficiently transfer electrons in QDSSCs. Further increase in the thickness was not observed when the deposition time was increased over 2 h. However, at 2.5 h of deposition, nanodendrites begin to form on the layer of PbS nanocrystals at uneven positions. Moreover when the deposition time increases from 2 h to 2.5 h, the nanocrystals disappeared. The PbS begins to peel off from the substrate when the deposition time increased to more than 2.5 h. When the deposition time was 2 h, the PbS nanocrystals had good adhesion to the FTO substrate. The degree of adhesion of the CE to the FTO substrate is a major factor for obtaining efficient QDSSCs.⁵⁰ If the materials do not stick to the FTO they could peel off from the FTO substrate, which may affect the performance of the QDSSCs.⁵¹

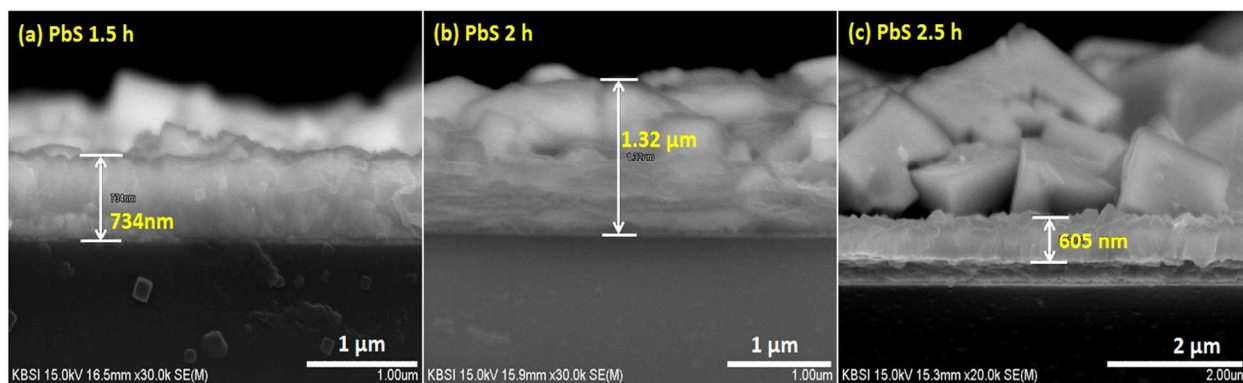


Fig. 4 Cross-section SEM images of PbS CEs for QDSSCs: (a) PbS 1.5 h, (b) PbS 2 h, and (c) PbS 2.5 h,

The fig.4 shows the thickness variation of PbS nanocrystals at various deposition times. For the preparation of PbS CEs, two main phenomena explain the formation of nanocrystals. First is the formation of crystals aggregates in the chemical solution related to nucleation, and second are the two growth mechanisms in CBD: ion-by-ion and cluster-by-cluster mechanisms. In CBD, these two mechanisms randomly occur and the aggregates form from the cluster-by-cluster mechanisms. The SEM images show that the average sizes of PbS nanocrystals are increased with the deposition time. Therefore, the range of deposition time from 1.5 h to 2 h is optimal for preparing high-quality cubic nanocrystals.

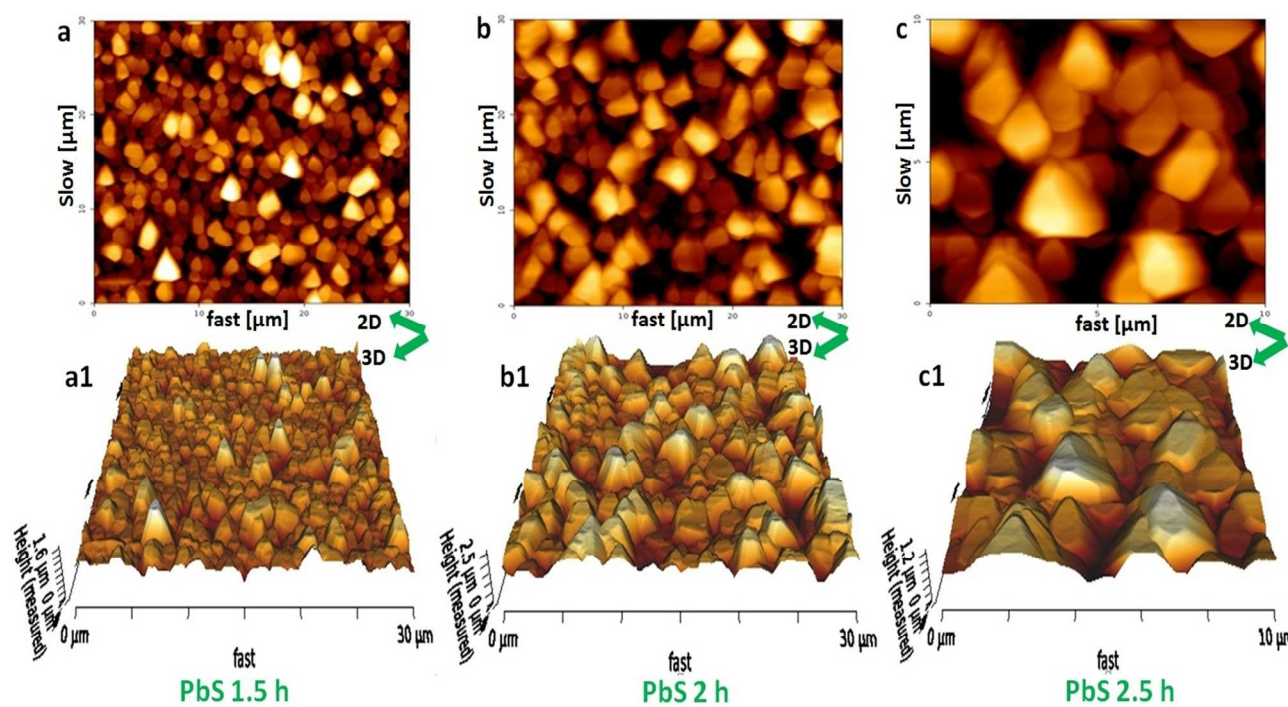


Fig. 5 2D (a, b, c) and 3D (a1, b1, c1) AFM images of PbS 1.5 h, PbS 2 h, and PbS 2.5 h CEs respectively.

Atomic force microscopy (AFM) is a promising technique to study the surface topography of thin films because it provides valuable information regarding the film growth mechanism, the shape and size of grains, and the surface roughness of the sample. Fig. 5 shows

2-dimensional (2D) and 3-dimensional (3D) AFM images of PbS thin films deposited on FTO substrate with various deposition times from 1.5 h to 2.5 h at constant temperature. The AFM images reveal a uniform surface roughness, a smooth surface, and good adherence to the substrate with narrow particle size distribution. The RMS values of all the CEs about 210 to 438 nm, respectively.

When the deposition time was 1.5 h, the PbS nanocrystals formed with small grains and uniform cubical shape could be observed on the substrate. The root mean square (RMS) roughness was about 210 nm with relatively low and narrow particle size distribution. The film deposited at 2 h has better morphology compared to that of 1.5 h and 2 h, and the surface roughness also increased. The roughness of PbS 2 h CE morphology is strongly affected by transition of active deposition mechanism during the course of the deposition. The RMS value gradually increases from 210 to 428 nm with increasing the deposition time from 1.5 h to 2.5 h. Das et al. reported that the rms roughness of their nanocrystalline PbS thin films was in the range of 11.8-43.7 nm.¹ Following this trend, the surface increases with the increasing the deposition time. This result suggests that when increasing the deposition from 1.5 h to 2 h, the film thickness increased and changed the nucleation, and the crystallization of the PbS thin films was improved. This is in good agreement with the XRD and SEM analysis.

When the deposition time was 2.5 h, the size of grains differs from that at 1.5 h and 2 h, indicating irregular growth rate of the grains. The variation of grains and grain boundaries is due to changes in crystallographic orientation, contaminants, and film quality. Therefore, 2 h results in larger specific surface area than 1.5 h and 2.5 h based on the RMS roughness and AFM images. The high surface at 2 h enhances the electrocatalytic activity for the CE in a polysulfide electrolyte system.⁵² This result also imply that the charge transfer resistance at the

CE/electrolyte interface would be lower in the case of 2 h. The deposition time of PbS 2 h CE offer more electrocatalytic activity sites for the reaction of the (S^{2-}/S_n^{2-}) redox couple in the polysulfide electrolyte and increase the area between the electrode and electrolyte. Therefore, the deposition time plays a vital role in the properties of PbS thin films and influenced the crystallization and surface roughness.

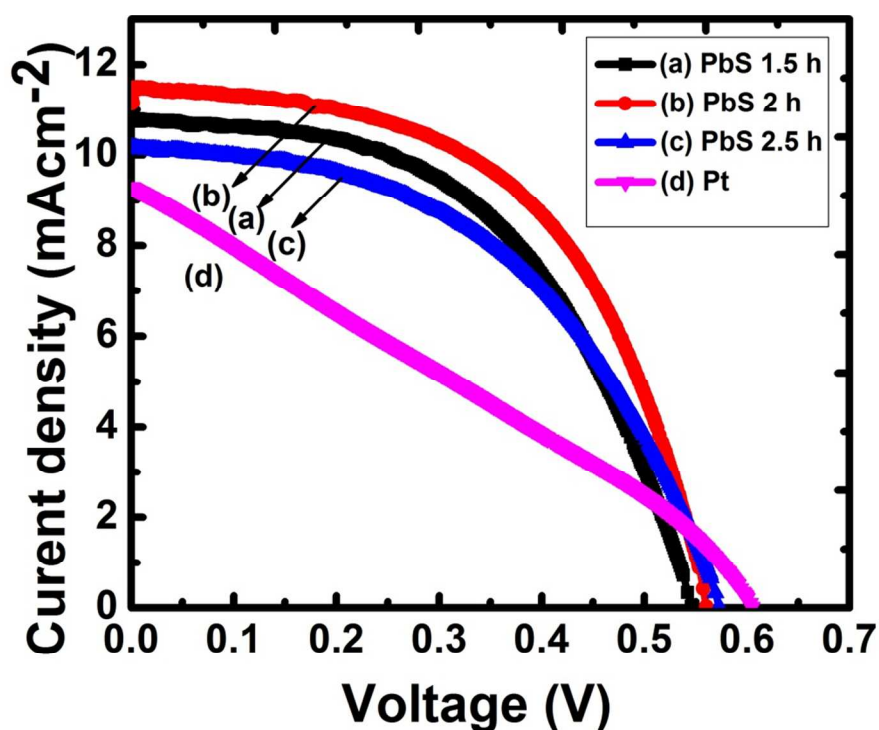


Fig. 6 Photocurrent-voltage (J-V) behavior for TiO₂/CdS/CdSe/ZnS QDSSCs based on PbS and Pt counter electrodes.

We also investigated the photovoltaic performance of PbS CE for QDSSCs. Fig. 6 presents the J-V characteristics obtained under A.M 1.5 sunlight illumination (100 mW cm^{-2}) for QDSSCs with PbS and Pt CE along with TiO₂/CdS/CdSe/ZnS as the photoanode. The QDSSC photovoltaic performance is determined by the short-circuit current density (J_{SC}), open-circuit

voltage (V_{oc}), fill factor (FF), and power conversion efficiency (η), which are summarized in table 2. For optimization of efficient PbS CEs, we prepared without using acetic acid as a reagent, and unfortunately, there was no visible coating on the FTO substrate. Using acetic acid in the preparation of PbS CEs, we observed semitransparency in the polysulfide electrolyte and good adherence to the FTO substrate.

The PbS CEs show better performance than the Pt CE. The Pt CE shows very poor performance in QDSSCs with J_{sc} , V_{oc} , and FF values of 10.20, 0.500, and 45.4, respectively, resulting in low energy conversion efficiency. These results are mainly due to the sulfides (S^{2-} , S_x^{2-}) adsorbing onto the Pt surface and poisoning it, which affects the electrocatalytic activity and reduces the FF and surface morphology.⁵³ For the PbS 2 h CE, the values of J_{sc} , V_{oc} , and FF significantly improved were 14.13, 0.610, and 55.7 respectively, and it had the best η of 3.48% in comparison with the PbS 1.5 h, PbS 2.5 h and Pt CEs. The efficiencies of the PbS 1.5 h and PbS 2.5 h were 3.02 and 2.85%, respectively. The improved performance of J_{sc} is mainly related to the low charge transfer resistance and more rapid rate of hole recovery at the PbS electrode/electrolyte interface. The hole recovery rate is an important factor in improving the energy conversion efficiency (η).⁵⁴⁻⁵⁸

The current-density mainly depends on the light harvesting efficiency, electron and hole injection efficiency, and charge collection efficiency.⁵⁹ The improved J_{sc} and efficiency of the PbS 2 h CE increase the charge transfer at the CE/electrolyte interface and reduces the internal resistance, recombination rates, and concentration gradients in the electrolyte,^{58, 30} resulting in improved FF , J_{sc} , and η . J_{sc} and the η of the PbS 2 h CE is much higher than that of other CEs, which demonstrates that the fabrication of PbS CEs through CBD is much better than that of other methods, such as hydrothermal or electrodeposition methods. The energy conversion

efficiency of the PbS CEs improves with up to 2 h of deposition and greatly decreases thereafter. From this result, we conclude that the PbS 2 h CE is the best substitute for Pt CEs.

A comparison with previously reported power conversion efficiency values of different CE materials (Graphene/PbS, PbS/En, Pb metal foil, CuS/PbS, PbS, ZnO/PbS) ^{60-65, 64} is depicted in fig. 7, which clearly shows that the our PbS 2 h CE has obtained greater performance and high electrocatalytic activity in comparison with different CE materials in aqueous polysulfide electrolyte. From the figure, the high performance of PbS 2 h CE results superior to that of different counter electrode materials for QDSSCs.

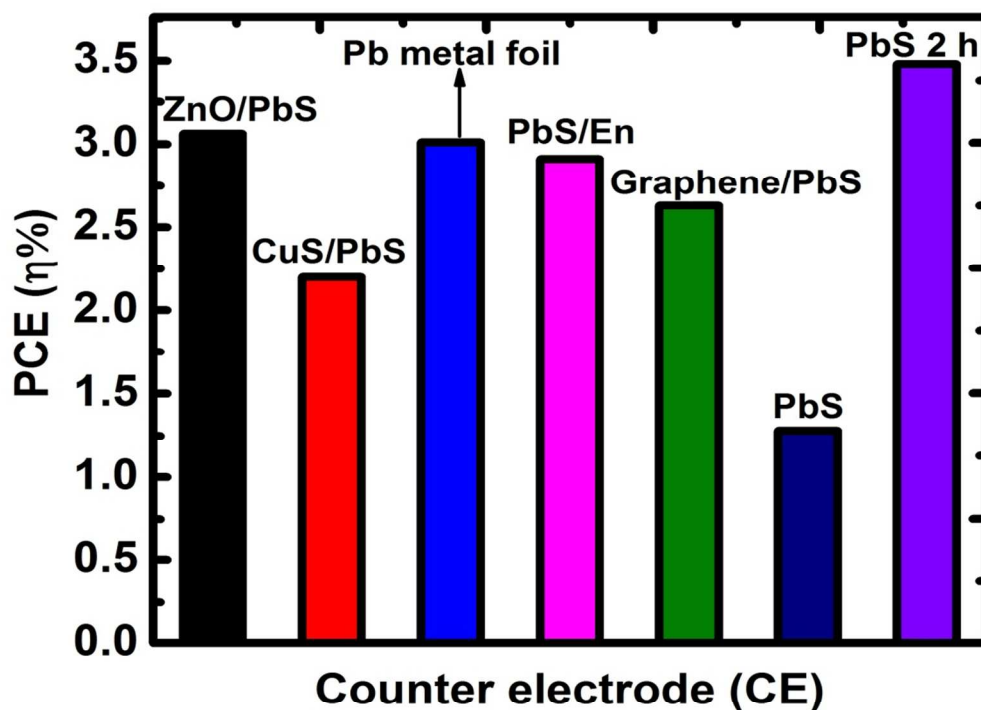


Fig. 7 Comparison of power conversion efficiency (PCE %) with different CE materials. PCE values for ZnO/PbS, CuS/PbS, Pb metal foil, PbS/En, Graphene/PbS, and PbS were taken from refs 60-65.

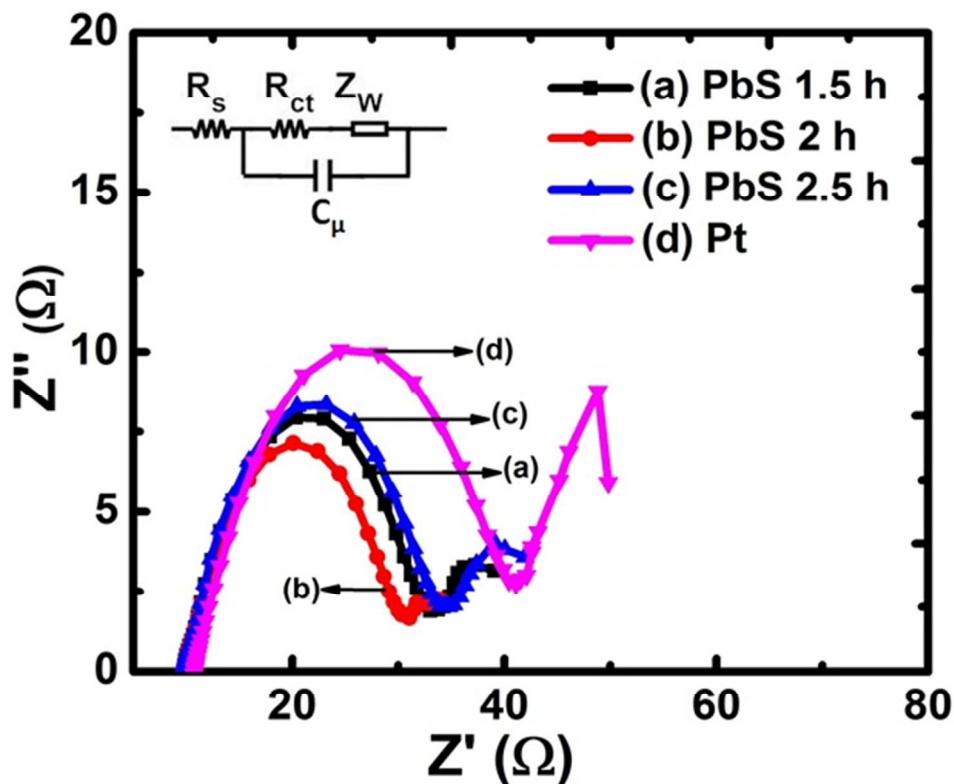
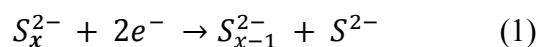


Figure 8. Nyquist (impedance) plots of PbS 1.5 h, PbS 2 h, and PbS 2.5 h and Pt symmetrical cells containing polysulfide electrolyte;

In QDSSCs, the CE and electrolyte play key roles in maintaining the regeneration cycle of QDs. Electrons have to be transferred to recover the holes of the QDs, which allow the QDs to be regenerated. Therefore, the oxidized species (i.e., S_x^{2-} ions) should be continuously reduced at the CE according to the following reaction:



EIS was used to investigate the catalytic properties of the symmetrical PbS CEs and the electron transport behavior, which is closely related to the electrocatalytic activity of the CEs in

reducing the polysulfide electrolyte. Fig. 8 shows the Nyquist plot obtained from parallel circuits with a resistor and capacitor connected in parallel⁶⁶ at open circuit bias potential in the frequency range of 100 mHz to 500 kHz and 0.6 V as well as the equivalent circuit used for fitting the impedance data of the PbS and Pt CEs at different deposition conditions. Z-view software was used to fit the parameters of the impedance spectra, which are shown in table 1. The Nyquist plot of the symmetrical cells consists of three parts. The equivalent circuit shows the Ohmic series resistance (R_s) determined in the high frequency region on the real axis where the phase is zero. The first semicircle represents the charge-transfer resistance (R_{ct}) with a constant-phase-angle element (CPE) at the CE/electrolyte interface in the middle frequency region, and the second semicircle denotes the Nernst diffusion impedance (Z_w) of the electrolyte in the low frequency region.

Table 1. EIS parameters extracted from fabricated symmetrical cells of PbS/PbS and Pt/Pt CEs, and the cells filled with a polysulfide electrolyte solution (1 M Na₂S, 2 M S, and 0.2 M KCl).

CEs	R_s (Ω)	R_{ct} (Ω)	CPE (μF)	Z_w (Ω)
PbS 1.5 h	9.92	23.38	17.04	6.12
PbS 2 h	9.58	20.28	25.29	3.86
PbS 2.5 h	9.97	24.29	16.46	8.11
Pt	11.12	29.91	16.22	9.02

R_{ct} directly relates to the electrocatalytic activity of the CE and controls the charge exchange between the CE and polysulfide electrolyte, while C_μ reflects the active surface area. The R_{ct} values of PbS 1.5 h, 2 h, 2.5 h and Pt CEs were 23.38, 20.28, and 24.29, 29.91

respectively. Because of corrosion of the Pt surface by various S species, the Pt CE shows a higher R_{ct} value than the PbS CE, which has improved electron transfer kinetics for S_n^{2-} reduction. In Contrast to the Pt, the lowest R_{ct} value of PbS 2 h CE suggests excellent electrocatalytic activity for S_x^{2-} ions in comparison with PbS 1.5 h, 2.5 h and Pt CEs. The low R_{ct} value of the PbS 2 h is a main factor for improving the power conversion efficiency, particularly in terms of FF at the CE/electrolyte interface. This result reduces the internal energy of the CE film and ensures full utilization of the PbS polycrystal cube structure (which is in good agreement with the SEM image).

Generally, a reduced R_{ct} would lead to high FF and greater power conversion efficiency.⁶⁷ The R_s values of the 1.5 h, 2 h, and 2.5 h PbS and Pt CE were 9.92, 9.58, 9.97, and 11.12, respectively. The low R_s values of PbS CE are due to the good adhesion of the CE to the FTO substrate and the sheet resistance of two electrodes with good conductivity. The C_μ values of the PbS 1.5 h, PbS 2 h, and PbS 2.5 h and Pt CEs were 17.04, 25.8, 16.6, and 16.22 μF , respectively. This reveals that the PbS CEs have higher CPE values than the Pt CE. The low recombination and larger electrochemical surface area of the PbS 2 h CE implies the availability of more catalytic sites. Therefore, a high C_μ value is a key factor for greater electrocatalytic activity.³⁹

In addition, the growth of PbS nanocrystals on the PbS 2 h CE is beneficial for the diffusion of the polysulfide electrolyte, which leads to much lower Z_w . The lower Z_w value (3.86) of the PbS 2 h is higher than that of the PbS 1.5 h, PbS 2.5 h and Pt CEs. The lower Z_w values of the PbS 2 h indicate sufficient electrocatalytic area for S_x^{2-} ions in the reduction reaction with improved electrolyte diffusion for mass transport of the electrons, which favors higher J_{SC} for QDSSCs. The Pt CE does not catalyze the reduction of polysulfide electrolyte

effectively, indicating poor performance in terms of low FF, which will affect the photovoltaic performance. We conclude from the impedance spectra of symmetrical cells that the PbS 2 h CE facilitates the penetration of electrolyte into the film and enables more electrochemical active sites for the S_x^{2-}/S^{2-} redox reaction.

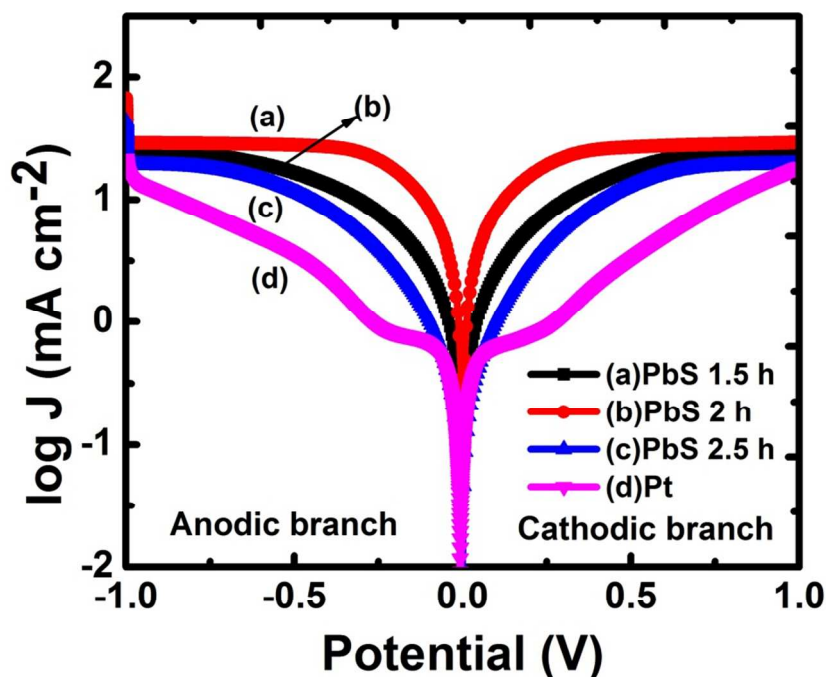


Fig. 9 Tafel polarization plot for PbS and Pt counter electrodes symmetrical cells

To further evaluate the interfacial charge transfer property of the S_x^{2-}/S^{2-} redox couple of PbS CEs, we used TAFEL polarization measurement with the same symmetrical cells used in the EIS analysis. Fig. 9 shows the Tafel measurement of the symmetrical cells of the PbS CEs and Pt CE under dark conditions with a scan rate of 10 mVs^{-1} as a function of the logarithmic current density (Log J) vs. potential (V). Theoretically, the Tafel polarization is mainly divided into three major parts, which consist of polarization, the Tafel zone and diffusion zones in the low, middle, and high potential areas, respectively. The figure presents

the electrocatalytic activities of CEs that can be evaluated from the exchange current density (J_0) and limiting diffusion current density J_{lim} obtained from the Tafel and diffusion zones. The limiting current density J_{lim} can be derived from the plot as a function of voltage, and the exchange current density (J_0) can be derived as the intercept of the extrapolated linear region of the anodic and cathodic branches when the voltage is zero. These two parameters are measures of the electrochemical catalytic activity of the PbS and Pt CEs. J_0 depends on the R_{ct} value obtained from the EIS analysis:

$$J_0 = \frac{RT}{nFR_{ct}} \quad (2)$$

where R is the gas constant, F is the Faraday constant, T is temperature, n is the number of electrons involved in the reduction of disulfide at the CE, and R_{ct} is the charge transfer resistance at the CE/electrolyte interface obtained from EIS spectra.

According to the Tafel plot, the PbS CEs clearly have higher slope values compared to the Pt CE. The PbS 2 h CE has higher J_0 values than the PbS 1.5 h, PbS 2.5 h and Pt CEs in the Tafel zone. This indicates better electrocatalytic activity for the polysulfide electrolyte redox couple and greater ability to reduce the polysulfide electrolyte at the CE/electrolyte interface. The improvement of the catalytic activity of PbS also increases the logarithmic current densities in the anodic and cathodic reduction of Tafel polarization. According to the equation, the PbS 1.5 h, PbS 2 h, and PbS 2.5 h CEs show greater J_{lim} values compared to the Pt CE, indicating that the PbS CEs have large diffusion coefficient (D) values that allow high diffusion velocity of the redox couple in the electrolyte:

$$D = |J_{lim}|/2nFC \quad (3)$$

Where D is the diffusion coefficient of the polysulfide, l is the electrolyte thickness, n is the number of electrons involved in the reduction of disulphide at the counter electrode, F is the Faraday constant and C is the polysulfide electrolyte concentration.

Due to high J_{lim} , the PbS CEs achieve good catalytic activity compared to Pt in the reduction of the electrolyte. When the deposition time was over 1 h, both J_0 and J_{lim} gradually increased, leading to better electrocatalytic activity and the highest power conversion efficiency of 3.46 %. This is in good agreement with Table 2 from the J-V analysis. The deposition time of 2 h leads to a much greater slope. The surface morphologies of the nanocrystal structured counter electrode thin films with particularly large surface can decrease the resistances of charge transfer, accelerate the diffusion of electrolyte and increase the electron life time, which are determining factors affecting the QDSSC performance. The increase in the slope and decrease in the charge transfer resistance in the EIS and Tafel plots show good consistency with the corresponding photovoltaic performance of PbS 2 h CE, which has the highest electrocatalytic activity in the reduction of the S_x^{2-}/S^{2-} couple for QDSSCs.

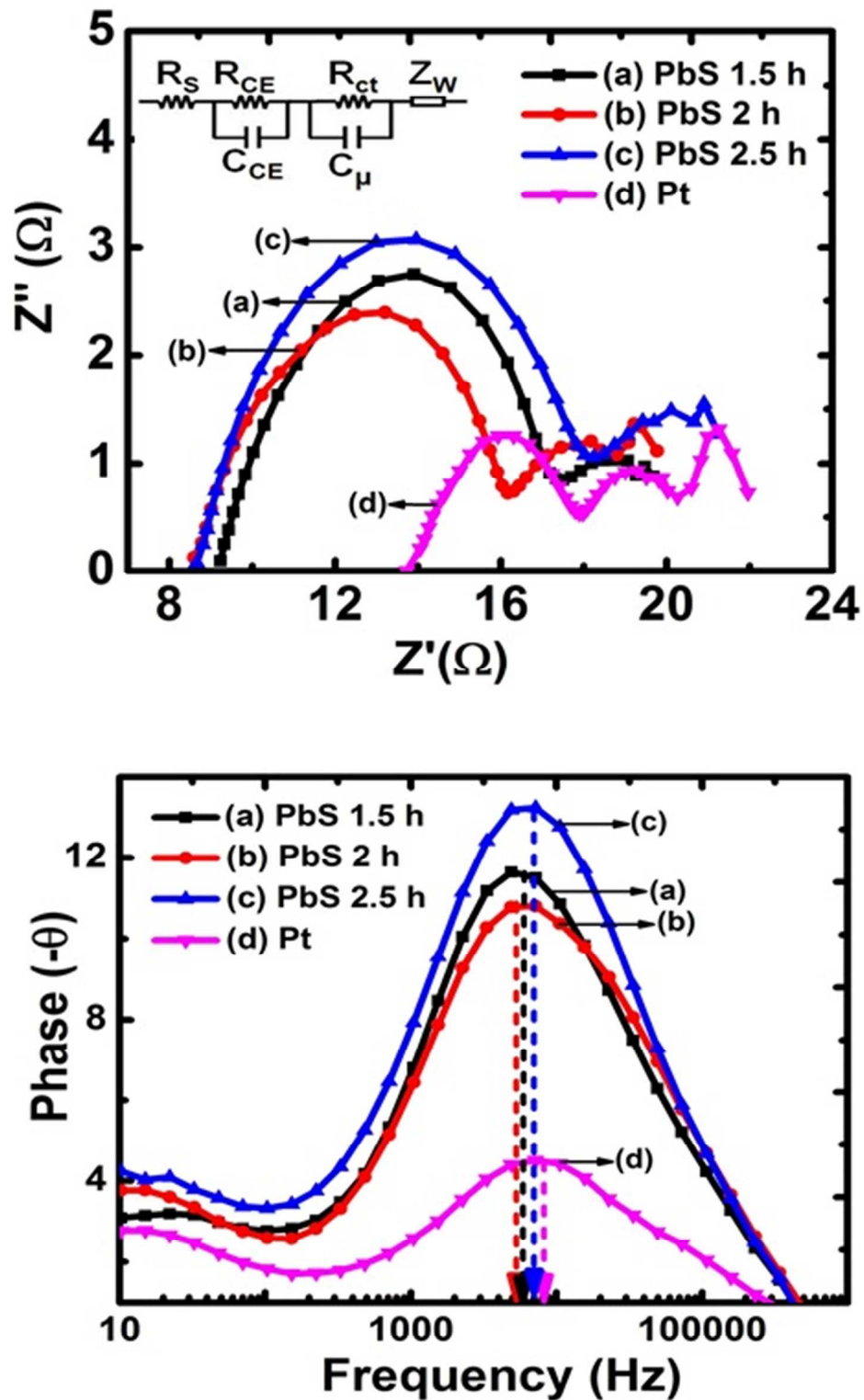


Fig. 10 Electrochemical impedance spectra of QDSSCs fabricated with PbS and Pt counter electrodes (A) the Nyquist plot with equivalent circuit, (B) the Bode plot.

To further understand the internal resistance, recombination properties, and interfacial charge-transfer kinetics of QDSSCs with different CEs, electrochemical impedance spectroscopy analysis was used under an illumination of 100 mW cm^{-2} . A 10-mV AC signal was applied for V_{oc} (under light conditions). The corresponding Nyquist plots are shown in Fig. 10 with the frequency range of 100 mHz to 500 kHz. Under illumination, electrons in the valence band have enough energy to inject into the QD-sensitized photoanode through the FTO substrate, and the photoanode is charged by transport of the injected electrons (in the conduction band). At the same time, some of the electrons in the conduction band of the photoanode recombine with the electrolyte. To classify these phenomena, Z-view software was used to analyze the impedance spectra from EIS analysis with an equivalent circuit consisting of two parallel RC circuits along with the Warburg impedance (Z_w), as shown in the figure.

Generally, the EIS spectra of QDSSCs show three semicircles in the frequency range of 100 mHz to 500 kHz. In the equivalent circuit diagram, a series resistance (R_s) was added to the circuit to describe the sheet resistance of the FTO/TiO₂, which represents the nonzero intercept on the real axis on the impedance plot. The first and second semicircles represent the charge transfer resistance at the CE/electrolyte interface and at the TiO₂/QD/electrolyte interface, respectively, with the corresponding chemical capacitance (C_μ), which represents the large number of photo-excited charge carriers in the conduction band of the photoanode resulting from very poor recombination. The third semicircle corresponds to the Warburg diffusion coefficient (Z_w) in the S_x^{2-}/S^{2-} redox electrolyte. The fitted values of the electrochemical parameters and electron lifetime are listed in table 2.

Table 2. Performance and EIS results of PbS and Pt CEs based on QDSSCs under one sun.

Parameter	V_{oc} (V)	J_{sc} (mA cm ⁻²)	FF	η (%)	R_s (Ω)	R_{CE} (Ω)	R_{ct} (Ω)	C_μ (μ F)	Z_w (Ω)	τ_n (ms)
PbS 1.5 h	0.545	10.79	0.51	3.02	9.18	7.01	1.75	2.04	1.40	2.82
PbS 2 h	0.560	11.20	0.55	3.48	8.58	4.42	2.6	4.63	1.21	3.04
PbS 2.5 h	0.572	10.7	0.49	2.85	8.61	8.3	2.52	2.42	1.68	2.22
Pt	0.604	9.29	0.28	1.58	13.72	8.94	1.30	0.10	3.15	1.59

The decreased first semi-circle shows the acceleration of the electron transfer at the CE/electrolyte interface. The R_{CE} values of the PbS 1.5 h, 2 h, 2.5 h and Pt CEs are 7.01, 4.42, 8.31, and 8.94, respectively. Compared to the PbS 1.5 h, 2.5 h and Pt CEs, the PbS 2 h CE has the lowest R_{CE} value, which indicates higher electrocatalytic activity than the other CEs. The R_{ct} , Z_w , and C_μ values of the PbS 2 h CE are 2.6, 1.21, and 4.63, respectively. The values for the Pt CE are 2.35, 3.15, and 0.10, respectively. The Pt CE has much higher values than the PbS, which means greater internal energy loss at the CE/electrolyte interface and leads to lower FF (0.28).⁶⁸ The PbS 2 h has high capacitance (C_μ) and greater surface area on the electrode, which causes low recombination. The high C_μ value (4.63 μ F) PbS 2 h sample shows superior to that of other CEs. The greater C_μ value suggests a high surface area of the electrode, which leads better electrocatalytic activity.⁶⁹ The small value Z_w (1.21 Ω) of the PbS 2 h CE indicates additional electrolyte diffusion with faster mass transport of electrons, resulting in increasing FF. R_{CE} and R_{ct} suggest that the PbS 2 h CE is the best CE for the reduction of the polysulfide-based redox couple in QDSSCs.

To support the EIS results, we can also estimate the electron lifetime (τ_n) in the PbS and Pt CEs for QDSSCs. The corresponding Bode phase plots for the PbS 1.5 h, 2 h, 2.5 h and Pt CEs are shown in Figure. The electron lifetime (τ_n) can be determined from the peak angular frequency in the Bode plot. The value of τ_n can be obtained according to the following equation:

$$\tau_n = 1/2\pi f_{max} \quad (5)$$

where f_{max} is the peak frequency in the mid frequency ranges.⁷⁰ As shown in the figure, the τ_n values of the PbS 1.5 h, 2 h, 2.5 h and Pt CEs are 2.82, 3.04, 2.22, and 1.59, respectively. When increasing the deposition time from 1.5 h to 2 h, the electron lifetime in the PbS CEs improves, which supports the lower recombination rate of injected electrons for reduction of the polysulfide electrolyte.⁷¹ f_{max} is inversely proportional to the electron lifetime of electrons, and the larger value of the PbS 2 h leads to a longer lifetime and faster diffusion rate.⁷² However, the higher τ_n value of the PbS 2 h suggests that the electrons have slower charge recombination in the polysulfide electrolyte, resulting in higher J_{SC} and enhanced energy conversion efficiency for the QDSSCs.⁷³

The Pt shows very low electron lifetime for the QDSSCs due to higher Z_w and higher recombination of the injected electrons with the polysulfide electrolyte, which results in an extreme loss of FF and reduced electron lifetime and affects the cell performance.⁷⁴ The EIS, Tafel, and J-V results suggest that the deposition time of PbS 2 h results in high catalytic activity in terms of increased J_{SC} and C_μ and decreased R_{ct} and Z_w , which will significantly improve the performance of QDSSCs.

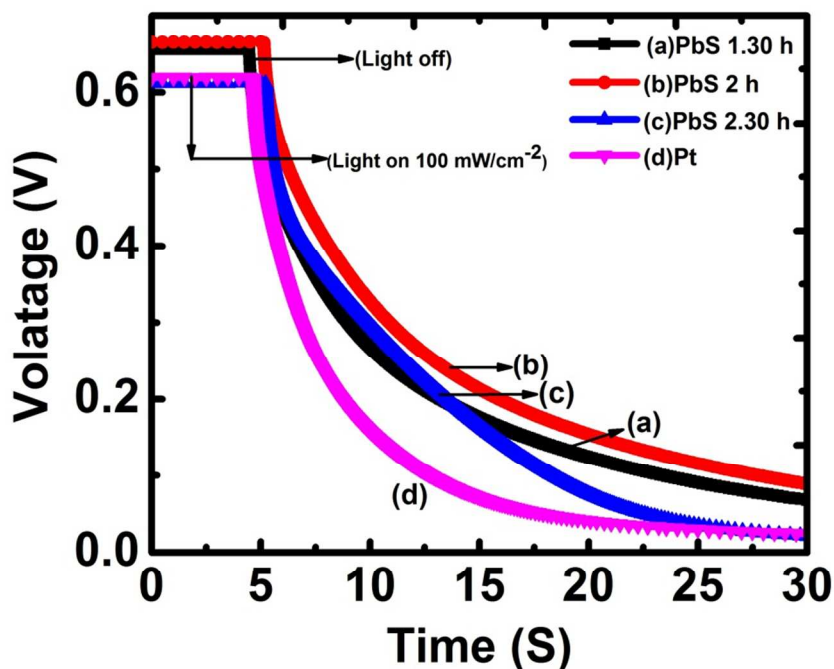


Figure 11. Open-circuit voltage-decay measurements after switching off the illumination of QDSSCs.

To further study the charge transport and recombination properties, the PbS CEs were investigated by open-circuit voltage decay (OCVD) measurements.⁷⁵ Fig. 11 shows the V_{oc} decay characteristics of QDSSCs with different CEs. The measurements were carried out as a function of time under open-circuit conditions. When the visible light illumination was removed, no electrons are transported through the external circuit due to the photoinduced electrons recombining with the electron acceptors in the electrolyte. Therefore, V_{oc} would follow an exponential curve during the recombination process. The rate of V_{oc} decay is directly proportional to the electron lifetime. The figure presents the OCVD traces measured for different deposition times of PbS and Pt CEs for QDSSCs. The electron lifetime can be calculated according to the following equation:

$$\tau_n = \frac{-k_{BT}}{e} \left[\frac{dV_{oc}}{dt} \right]^{-1} \quad (4)$$

where $k_B T$ is the thermal energy, e is the positive elementary charge, and dV_{oc}/dt is the derivative of V_{oc} .

It is clear that the QDSSCs based on the PbS 2 h CE have the slowest V_{oc} decay rate compared to the Pt CE. This suggests slower recombination kinetics and longer electron lifetime in the PbS 2 h. The plot for Pt shows the fastest voltage decay rate, indicating the largest recombination rate. Based on the QD amounts, light-scattering ability, electron transport, and recombination, the QDSSCs with the PbS 2 h achieved the highest PCE (3.48%) with a J_{sc} of 11.20, V_{oc} of 0.560, and FF of 0.55 under simulated AM 1.5 G one-sun (100 mW cm^{-2}) illumination.

The photovoltaic performances of the QDSSCs with the PbS CEs were compared based on the charge-transfer resistance at the CE/electrolyte interface, as shown in Fig. 12(b). Fig. 12(b) shows that the PbS 2 h CE provides a lower charge-transfer resistance (R_{ct}) at the CE/electrolyte interface, which is lower than that of PbS 1.5 h and PbS 2.5 h, and several orders of magnitude lower than that of the Pt CE. The lower R_{ct} in PbS 2 h CE suggests much enhancement of the charge transfer, which would improve the electron flow from the external circuit to the PbS/electrolyte interface. The lower R_{ct} value of PbS 2 h shows the superior photovoltaic performance than the PbS 1.5 h, PbS 2.5 h and Pt CEs. Higher photovoltaic performance and low internal resistance were observed for the PbS 2 h CE, which is in accordance with the solar cell performance results.

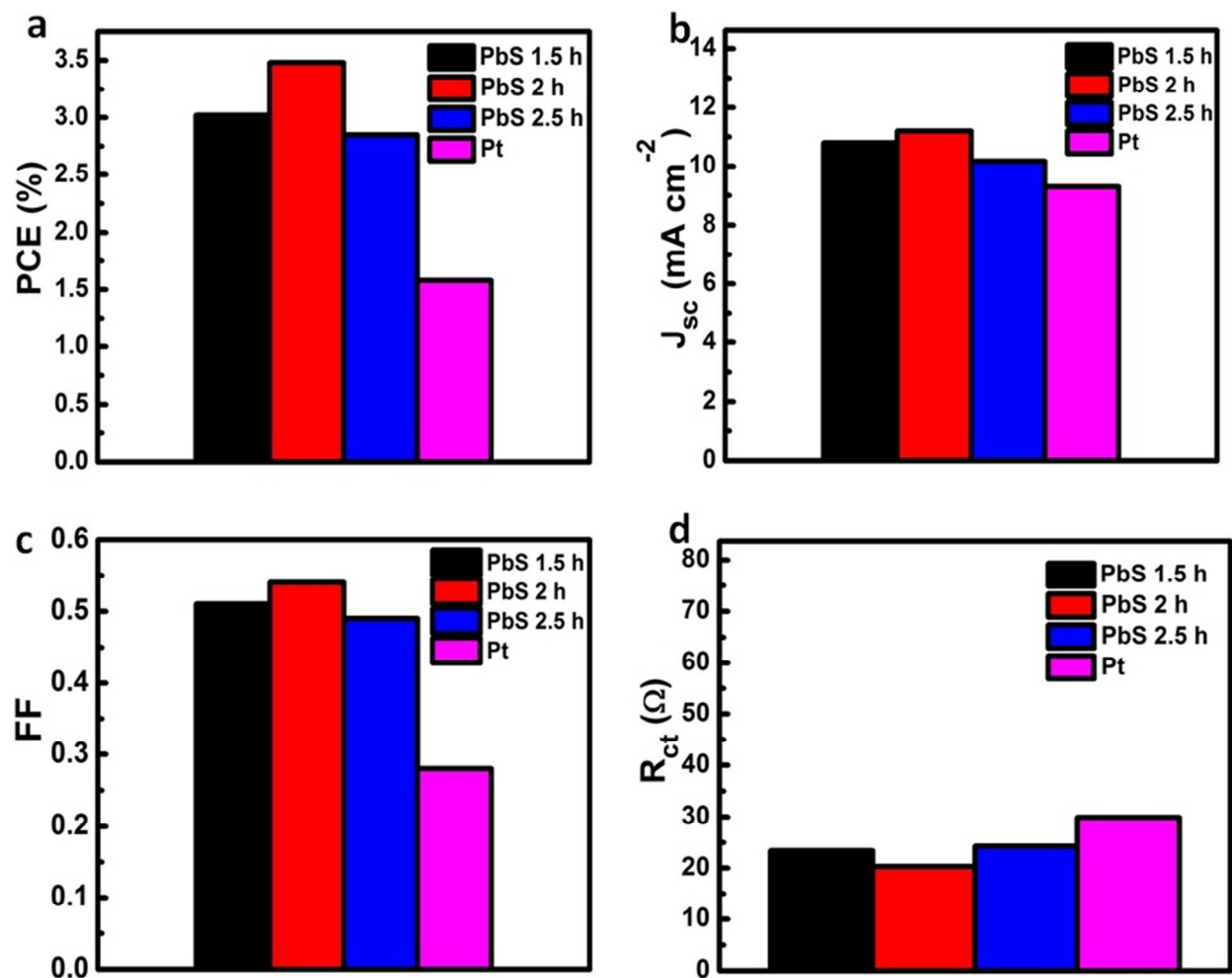


Fig. 12 Performance comparison between different FTO porous film-supported metal sulfide PbS CEs and Pt CE: (a) PCE, (b) J_{SC} (c) R_{ct} , and (d) FF.

Conclusion

We have demonstrated a simple and cost-effective approach to synthesizing high-quality PbS nanocrystals using CBD in the presence of acetic acid at various deposition times. To the best of our knowledge, this is the first time reporting the fabrication of horizontally aligned PbS CEs with improved cube-shaped nanocrystal morphology on FTO substrate and their application in QDSSCs. The size and shape of the PbS nanocrystals can be easily

controlled by varying the reaction time. The improved performance of the PbS 2 h CE in QDSSCs under one-sun illumination (AM 1.5, 100 Mw cm⁻²) yielded high power conversion efficiency (3.48 %), which is higher than those of the PbS 1.5 h CE (3.02 %), PbS 2.5 h CE (2.85%), and Pt (1.58%) CEs. The surface energy of the PbS 2 h CE can be controlled by the concentration of acetic acid, in contrast to the PbS 1.5 h and 2.5 h CEs. The concentration of acetic acid plays an important role in deciding the size and shape of the PbS nanocrystals in the nucleation and growth process.

In EIS analysis, the PbS 2 h CE shows the lowest charge transfer resistance (20.28 Ω) compared to the Pt CE (29.91 Ω) at the polysulfide/electrolyte interface. Moreover, the PbS 2 h CE has a longer electron lifetime of 3.04 ms. The improved photovoltaic performance is mainly attributed to the surface energy of the PbS 2 h, modified surface morphology, faster electron transport, and lower electron recombination rate. These results indicate that CBD can be used to selectively deposit layers on organic films and to control the surface morphology, size, and shape of PbS nanocrystals by varying the reaction conditions. We anticipate that this method can be applied to other substrates for potentially high-efficiency QDSSCs, Perovskite solar cells, LEDs, and infrared solar cells.

Acknowledgements

This research was supported by Basic Science Research Program through the National Research Foundation of Korea (NRF) funded by the Ministry of Education, Science and Technology (2011-0014437). We also thankful to KBSI for SEM, AFM and XRD measurements.

References:

1 Y. Sun, Q. Wu, and G. Shi, *Energy Environ. Sci.*, 2011, **4**, 1113–1132. NiCo₂S₄

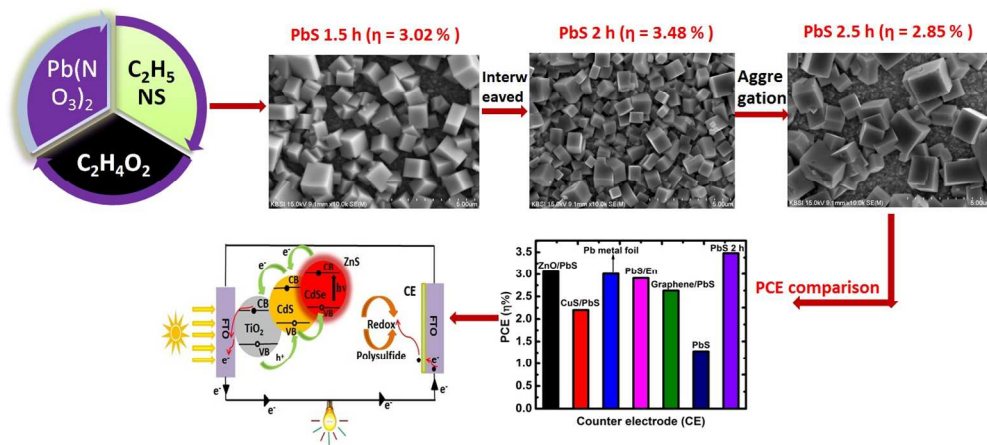
- 2 L. J. Xie, J. F. Wu, C. M. Chen, C. M. Zhang, L. Wan, J. L. Wang, Q. Q. Kong, C. X. Lv, K. X. Li, and G. H. Sun, *J. Power Sources.*, 2013, **242**, 148–156.
- 3 W. Du, R. Liu, Y. Jiang, Q. Lu, Y. Fan, and F. Gao, *J. Power Sources.*, 2013, **227**, 101–105.
- 4 P. V. Kamat, *J. Phys. Chem. C.*, 2008, **112**, 18737.
- 5 Z. S. Yang, C. Y. Chen, P. Roy and H. T. Chang, *Chem. Commun.*, 2011, **47**, 9561.
- 6 P. Chen, L. Gu and X. B. Cao, *CrystEngComm.*, 2010, **12**, 3950.
- 7 L. M. Peter, K. G. U. Wijayantha, D. J. Riley and J. P. Waggett, *J. Phys. Chem. B.*, 2003, **107**, 8378.
- 8 S. Buhbut, S. Itzhakov, E. Tauber, M. Shalom, I. Hod, T. Geiger, Y. Garini, D. Oron and A. Zaban, *ACS Nano.*, 2010, **4**, 1293.
- 9 A. J. Nozik, *Phys. E.*, 2002, **14**, 115–120.
- 10 S. Gimeenez, I. Mora-Seroo, L. Macor, N. Guijarro, T. Lana-Villarreal, R. Goomez, L. J. Diguna, Q. Shen, T. Toyoda, and J. Bisquert, *Nanotechnology.*, 2009, **20**, 295204.
- 11 S. C. Lin, Y. L. Lee, C. H. Chang, Y. J. Shen, and Y. M. Yang, *Appl. Phys. Lett.*, 2007, **90**, 143517.
- 12 I. Robel, V. Subramanian, M. Kuno, and P. V. Kamat, *J. Am. Chem. Soc.*, 2006, **128**, 2385–2393.
- 13 P. K. Santra, and P. V. Kamat, *J. Am. Chem. Soc.*, 2012, **134**, 2508–2511.
- 14 H. Lee, M. K. Wang, P. Chen, D. R. Gamelin, S. M. Zakeeruddin, M. Graetzel, M. K. Nazeeruddin, *Nano Lett.*, 2009, **9**, 4221–4227.
- 15 L. W. Chong, H. T. Chien, and Y. L. Lee, *J. Power Sources.*, 2010, **195**, 5109–5113.
- 16 Y. H. Lee,; S. H. Im, J. H. Rhee, H. Lee, and S. Seok, *ACS Appl. Mater. Interfaces.*, 2010, **2**, 1648–1652.

- 17 T. L. Li, Y. L. Lee and H. Teng, *Energy Environ. Sci.*, 2012, **5**, 5315.
- 18 K. P. Kadlag, P. Patil, M. J. Rao, S. Datta and A. Nag, *CrystEngComm.*, 2014, **16**, 3605.
- 19 K. Zhao, Z. Pan, I. Mora-Sero, E. Canovas, H. Wang, Y. Song, X. Gong, J. Wang, M. Bonn, J. Bisquert, and X. Zhong, *J. Am. Chem. Soc.*, 2015, **137**, 5602–5609
- 20 M.S. Faber, K. Park, M. Caban-Acevedo, P.K. Santra, and S. Jin, *J. Phys. Chem. Lett.*, 2013, **4**, 1843-1849.
- 21 P.V. Kamat, *Acc. Chem. Res.*, 2012, **45**, 1906-1915.
- 22 V. Chakrapani, D. Baker, and P.V. Kamat, *J. Am. Chem. Soc.*, 2011, **133**, 9607-9615.
- 23 Z. Yang, C.Y. Chen, C.W. Liu, and H.T. Chang, *Chem. Commun.*, 2010, **46**, 5485-5487.
- 24 X. Song, M. Wang, Y. Shi, J. Deng, Z. Yang, and X. Yao, *Electrochim. Acta.*, 2012, **81**, 260-267.
- 25 J.G. Radich, R. Dwyer, and P.V. Kamat, *J. Phys. Chem. Lett.*, 2011, **2**, 2453-2460.
- 26 M. Shalom, S. Dor, S. Ruhle, L. Grinis and A. Zaban, *J. Phys. Chem. C.*, 2009, **113**, 3895.
- 28 C. Shen, L. D. Sun, Z. Y. Koh and Q. Wang, *J. Mater. Chem. A.*, 2014, **2**, 2807.
- 29 Z. Yang, C. Y. Chen, C. W. Liu, C. L. Li and H. T. Chang, *Adv. Energy Mater.*, 2011, **1**, 259.
- 30 H. N. Chen, L. Q. Zhu, H. C. Liu and W. P. Li, *J. Phys. Chem. C.*, 2013, **117**, 3739.
- 31 Z. Tachan, M. Shalom, I. Hod, S. Ruhle, S. Tirosh and A. Zaban, *J. Phys. Chem. C.*, 2011, **115**, 6162.
- 32 J. N. Freitas, A. S. Goncalves and A. F. Nogueira, *Nanoscale.*, 2014, **6**, 6371.
- 33 D. H. Youn, M. Seol, J. Y. Kim, J. W. Jang, Y. Choi, K. Yong and J. S. Lee, *ChemSusChem.*, 2013, **6**, 261.
- 34 M. Seol, D. H. Youn, J. Y. Kim, J. W. Jang, M. Choi, J. S. Lee and K. Yong, *Adv. Energy Mater.*, 2014, **4**, 1300775.

- 35 T. H. Thanh, D. H. Thanh and V. Q. Lam, *Adv. OptoElectron.*, 2014, **2014**, 397681.
- 36 G.S. Paul, J.H. Kim, M. S. Kim, K. Do, J. Ko, J. S. Yu, *ACS Appl. Mater. Interfaces.*, 2012, **4** 375-381.
- 37 F. Hao, P. Dong, J. Zhang, Y. Zhang, P.E. Loya, R.H. Hauge, J. Li, J. Lou, H. Lin, *Sci. Rep.*, 2012, **2**, 368.
- 38 M. H. Yeh, C. P. Lee, C. Y. Chou, L. Y. Lin, H. Y. Wei, C. W. Chu, R. Vittal, K. C. Ho, *Electrochim. Acta.*, 2011, **57**, 277–284.
- 39 V. Gonzalez-Pedro, X. Xu, I. Mora-Sero, and J. Bisquert, *ACS Nano.*, 2010, **4**, 5783–5790.
- 40 G.Hodes, J. Manassen, and D. Cahen, *J. Electrochem. Soc.*, 1980, **127**, 544-549.
- 41 D. Liu, and P. V. Kamat, *J. Phys. Chem.*, 1993, **97**, 10769-10773.
- 42 Y. F. Nicolau, *Appl. Surf. Sci.*, 1985, **22/23**, 1061-1074.
- 43 S.S. Kalanur, S.Y. Chae, and O.S. Joo, *Electrochim. Acta.*, 2013, **103**, 91-95.
- 44 K. R. Gopidas, M. Bohorquez, and P. V. Kamat, *J. Phys. Chem.*, 1990, **94**, 6435-6440.
- 45 R. S. Mane, and C. D. Lokhande, *Mater. Chem. Phys.*, 2000, **65**, 1-31.
- 46 P. Parand, M. Samadpour, A. Esfandiar, and A. Irajzi Zad, *ACS Photonics.*, 2014, **1**, 323–330.
- 47 Y. Chen, X. Zhang, Q. Tao, W. Fu, H. Yang, S. Su, Y. Mu, L. Zhoua and M. Li, *RSC Adv.*, 2015, **5**, 1835–1840.
- 48 R. Vogel, K. Pohl, and H. Weller, *Chem. Phys. Lett.*, 1990, **174**, 241-246.
- 49 N. Guijarro, J. M. Campin, Q. Shen, T. Toyoda, T. Lana-Villarreal and R. Gomez, *Phys. Chem. Chem. Phys.*, 2011, **13**, 12024–12032.
- 50 A. Hauch, and A. Georg, *Electrochimica Acta.*, 2001, **46**, 3457-3466.
- 51 V. C. pani, D. Baker, P.V. Kamat, *J. Am. Chem. Soc.*, 2011, **133**, 9607-9615.

- 52 (a) S. Q. Fan, B. Fang, J. H. Kim, J. J. Kim, J. S. Yu, and J. Koa, *Appl. Phys. Lett.*, 2010, **96**, 063501-1.
- (b) J. G. Chena, H. Y. Weib, and K.C. Ho, *Sol. Energy Mater. Sol. Cells.*, 2007, **91**, 1472-1477.
- 53 V. Gonzalez-Pedro, X. Xu, I. Mora-Sero, and J. Bisquert, *ACS Nano.*, 2010, **4**, 5783–5790.
- 54 H. Joong Lee, P. Chen, S. Moon, F. Sauvage, K. Sivula, T. Bessho, D. R. Gamelin, P. Comte, S. M. Zakeeruddin, S. Seok, M. Gratzel, and Md. K. Nazeeruddin, *Langmuir.*, 2009, **25(13)**, 7602–7608.
- 55 L. E. Brus, *J. Chem. Phys.*, 1984, **80 (9)**, 094403.
- 58 L. J. Diguna, Q. Shen, J. Kobayashi, and T. Toyoda, *Appl. Phys. Lett.*, 2007, **91**, 023116.
- 57 L. Yuh-Lang, and C. Chi-Hsiu, *J. Power Sources.*, 2008, **185**, 584–588.
- 58 L. Cheng-Yu, T. Chiao-Yi, Li. Tzung-Luen, L. Yuh-Lang and H. Teng, *J. Mater. Chem. A.*, 2013, **1**, 1155–1162.
- 59 David B. Mitzi, *J. Chem. Soc. Dalton Trans.*, 2001, 1.
- 60 X. Song, M. Wang, J. Deng, Y. Ju, T. Xing, J. Ding, Z. Yang, and J. Shao, *J. Power Sources.*, 2014, **269**, 661-770.
- 61 M. Eskandari, V. Ahmadi, and R. Ghahary, *Electrochim.Acta.*, 2015, **151**, 393-398.
- 62 Z. Tachan, M. Shalom, I. Hold, S. Ruhle, S. Tirosh, and A. Zaban, *J. Phyc. Chem. C.*, 2011, **115**, 6162-6166
- 63 Y. Chen, X. Zhang, Q. Tao, W. Fu, H. Yang, S. Su, Y. Mu, L. Zhoua and M. Li, *RSC Adv.*, 2015, **5**, 1835–1840
- 64 P. Parand, M. Samadpour, A. Esfandiar, and A. Iraj Zad, *ACS Photonics.*, 2014, **1**, 323–330.
- 65 J. B. Zhang, F. Y. Zhao, G. S. Tang, and Y. Lin, *J Soli State Electrochem.*, 2013, **17**, 2909-2915

- 66 L. Guldbrand, B. JOnsson, H. Wennerstrom, and P. Linse, *J. Chern. Phys.*, 1984, **80** (5).
- 67 X. Fang, T. Ma, G. Guan, M. Akiyama, T. Kida, E. Abe, *J. Electroanal. Chem.*, 2004, **570**, 257-263
- 68 Q. Wang, J. E. Moser, and M. Gratzel, *J. Phys. Chem. B.*, 2005, **109**, 14945-14953.
- 69 R. Kern, R. Sastrawan, J. Ferber, R. Stangl, and J. Luther, *Electrochim. Acta.*, 2002, **47**, 4213–4225
- 70 N. G. Park, M. G. Kang, K. M. Kim, K. S. Ryu, and S. H. Chang, *Langmuir.*, 2004, **20**, 4246-4253.
- 71 C. Y. Lin, C. Teng, T. Li, Y. L. Leea, and H. Teng, *J. Mater. Chem. A.*, 2013, **1**, 1155-1162.
- 72 X. Hou, Y. Hu, H. Jiang, J. Huo, Y. Li and C. Li, *J. Mater. Chem. A.*, 2013, **1**, 13814-13820.
- 73 C. Hsin-Wei, L. Chih-Peng, H. Hou-Sheng, C. Jian-Ging, R. Vittal, L. Chia-Yu, C.W. Kevin Wu and H. Kuo-Chuan, *Chem. Commun.*, 2011, **47**, 8346-8348.
- 74 J.D. Chena, H.Y. Wei, and K. C. H. Sol. Energy Mater. Sol. Cells., 2007, **91**, 1472.
- 75 A. Zaban, M. Greenshtein, and J. Bisquert, *ChemPhysChem.*, 2003, **4**, 859.



411x183mm (96 x 96 DPI)